2026 IEEE International Conference on Robotics and Automation (ICRA 2026)
June 1-5, 2026. Vienna, Austria

Bio-Inspired Liquid Crystal Elastomer Suction Actuator for Intelligent Robotic Grasping

Shen Gao, Yongzheng Luo, Mingjun Tang, Yue Wang*, Tao Yue, *Member, IEEE*

***Abstract*— Grasping operations constitute a fundamental mechanism for robotic interaction with the environment and task execution, playing a critical role in logistics, unmanned systems, and complex terrain exploration. Conventional rigid grasping devices are often bulky and exhibit limited adaptability and controllability in unstructured environments. Suction-based grippers offer improved environmental compliance but typically require extensive tubing and vacuum pumps, constraining their integration into lightweight and soft robotic platforms. Inspired by octopus suction cups, recent bioinspired designs have leveraged geometrical optimization and flexible materials to enhance adhesion, yet most still rely on external actuation or complex vacuum systems, failing to replicate the rapid, reversible adhesion achieved through muscular contraction. To address this challenge, we present a bioinspired suction actuator based on liquid crystal elastomer (LCE), exploiting their reversible anisotropic–isotropic phase transition under thermal stimuli to dynamically modulate the cavity volume and generate controllable negative pressure. The proposed design closely emulates octopus muscle mechanics while significantly simplifying structural complexity, achieving a combination of light weight, compliance, and programmability. Experiments demonstrate stable adhesion of 30 kPa on glass over 300 cycles, with rapid and reliable attachment/detachment under varying conditions, highlighting potential applications in climbing robots, aerial grasping, and underwater exploration.**

I. Introduction

Grasping mechanisms represent the core interface through which robots interact with their environments, and their performance directly determines the reliability, efficiency, and adaptability of robotic operations in logistics, unmanned systems, and complex environments [1,2]. Conventional rigid grippers, while mechanically robust and effective for handling regular objects, often lack adaptability in unstructured or dynamic scenarios, making it difficult to stably manipulate soft, fragile, or irregular targets. This limitation hinders their integration into lightweight and flexible robotic platforms. Suction-based grasping devices offer advantages in terms of environmental adaptability and the ability to operate on diverse surface conditions, thereby partially overcoming the shortcomings of rigid designs [2-5]. However, they typically rely on bulky vacuum pumps and intricate pneumatic circuits, which not only increase energy consumption and maintenance requirements but also render the system heavy and limit its response speed. These drawbacks become particularly pronounced in mobile, aerial, and underwater robots, where stringent demands for lightweight design and system integration prevail. To address these challenges, researchers have turned to novel actuation principles, bio-inspired architectures, and smart responsive materials, aiming to achieve controllable, lightweight, rapid, and reversible grasping without external assistance. Such advances hold promised for enabling efficient robotic operation in complex and dynamic environments.

Through long-term evolution, organisms in nature have developed highly specialized structures and functions that enable remarkable adaptability to diverse environments, offering abundant inspiration for robotic design. For instance, geckos rely on hierarchically structured setae at the micro- and nanoscale, which exploit van der Waals forces to achieve efficient, reversible adhesion and climbing on smooth walls [6,7]; barnacles secrete protein-rich bio-adhesives that allow them to remain firmly attached in wet and complex underwater conditions [8]; while octopuses utilize muscular contraction of their suction cups to modulate cavity volume, thereby generating reversible and precise negative pressure for stable and versatile grasping across different surfaces and environments [9-11]. Inspired by these biological strategies, bio-inspired grasping research has gradually advanced through mimicking geometrical structures, integrating flexible materials, or emulating muscle-driven mechanisms to enhance environmental adaptability and operational performance. Although existing octopus-inspired suction devices have demonstrated notable progress in structural design and compliance, particularly outperforming rigid grippers in grasping irregular or wet surfaces, most approaches still depend on external vacuum pumps, complex tubing, or mechanical actuators. Such reliance hinders the realization of reversible, lightweight, and fully integrated suction, thereby limiting their applicability in mobile, aerial, and underwater robotic systems. Consequently, identifying a mechanism that enables direct modulation of cavity volume at the material level has emerged as a critical challenge. Against this backdrop, liquid crystal elastomer (LCE), with its thermally induced reversible phase transitions and highly programmable deformation behaviors, provides a promising material pathway for constructing bio-inspired suction systems without external assistance [12].

Liquid crystal elastomer (LCE) is an intelligent material capable of undergoing reversible phase transitions in response to external stimuli. Owing to its unique molecular architecture and programmable responsiveness, it has emerged as a promising candidate in recent years [13-16]. LCE is

This work was supported by the grants from the National Natural Science Foundation of China (No. 62303290, 52305325, 62373235), Shanghai Magnolia Talent Program Pujiang Project (No. 23PJD036)

(Shen Gao, Yongzheng Luo, Mingjun Tang, Yue Wang) School of Future Technology, Shanghai University, Shanghai, China (e-mail: gaoshen@shu.edu.cn, luoyongzheng@shu.edu.cn, tmj@shu.edu.cn, yue_wang@shu.edu.cn)

(Shen Gao, Tao Yue) School of Mechatronic Engineering and Automation, Shanghai University, Shanghai, China (e-mail: gaoshen@shu.edu.cn, tao_yue@shu.edu.cn)

*Corresponding author

synthesized via click chemistry, where liquid-crystalline mesogens are crosslinked with chain extenders to form a flexible polymer network. After polymerization, applying a uniaxial aligning force induces molecular orientation, which is then fixed through photopolymerization initiated by UV irradiation, resulting in anisotropic LCE [17]. When exposed to external stimuli—primarily thermal input—the anisotropic state reverts to an isotropic state, accompanied by macroscopic contraction or expansion. This dual characteristic, combining the ordered orientation of liquid crystals with the elasticity of polymer networks, enables LCE to exhibit pronounced, reversible, and controllable deformation under light [18], heat [19], electric [20], or magnetic fields [21]. Under thermal stimulation, LCE undergoes an anisotropic-to-isotropic phase transition, accompanied by substantial volume modulation and complex shape reconfiguration. This property aligns closely with the biological mechanism of octopus suckers, which rely on muscular contraction to modulate chamber volume and generate negative pressure for adhesion. Unlike conventional suction devices that depend on bulky vacuum pumps and complex tubing, LCE-based actuators directly regulate chamber volume through intrinsic phase-transition-driven deformation, thereby simplifying system architecture and enhancing light weight and compliance. Recent studies have highlighted the potential of LCE in bioinspired structures, programmable morphing, soft robotics, and miniaturized devices. For instance, Zhu et al. fabricated a sandwich-structured composite consisting of silver nanowires, PDMS/CB, and oriented LCE. Joule heating of the silver nanowires induced localized thermal stimulation, driving LCE from anisotropic to isotropic states, leading to directional contraction. By selectively heating different regions, the system achieved sequential bending and stretching, mimicking caterpillar locomotion with controllable motion direction and amplitude—promising for confined-space exploration [22]. Yang et al. developed a photo-thermally powered miniature jumping robot inspired by springtails. By incorporating carbon nanotubes during LCE synthesis, infrared irradiation triggered a photothermal effect that induced isotropic transition and structural unfolding of a predesigned folded geometry, generating sufficient force for self-propelled jumping [23]. Lv. and colleagues drew inspiration from spider silk spinning and developed an efficient LCE bio-fabrication platform to produce fibrous LCE with muscle-like properties, demonstrating strong potential in soft robotics, wearable exoskeletons, and rehabilitation devices [24]. Nevertheless, most existing studies have primarily focused on motion control and actuation behaviors based on bulk contraction of LCE, while exploration of function-driven applications, such as bioinspired suction-based adhesion and grasping, remains relatively limited. Fully exploiting the thermally induced actuation capability of LCE to construct lightweight, reversible, and efficient bioinspired suction systems thus represents a critical challenge and research opportunity.

In this work, we propose an octopus-inspired thermally actuated suction cup based on liquid crystal elastomer (LCE), designed for applications such as object grasping and wall climbing. A key innovation lies in the development of a synthesis strategy that imparts programmable anisotropy to LCE. Specifically, we fabricated a negative mold of the suction cup using high-resolution photocuring 3D printing. The mold geometry was then imprinted onto the surface of isotropic LCE, followed by UV-initiated polycondensation to fix the transferred pattern, thereby yielding customized, patterned anisotropic LCE. We systematically compared suction cups composed of LCE (S-LCE) with different internal geometries to determine the optimal structure and dimensions. The adhesion performance of S-LCE was quantitatively evaluated, and the optimized design was further integrated into a robotic arm for grasping tasks. Experimental results demonstrate that S-LCE exhibits excellent adhesion and grasping capabilities, while offering distinct advantages in terms of lightweight system integration. These findings highlight the significant potential of S-LCE for execution tasks in unmanned systems requiring efficient and adaptable grasping solutions.

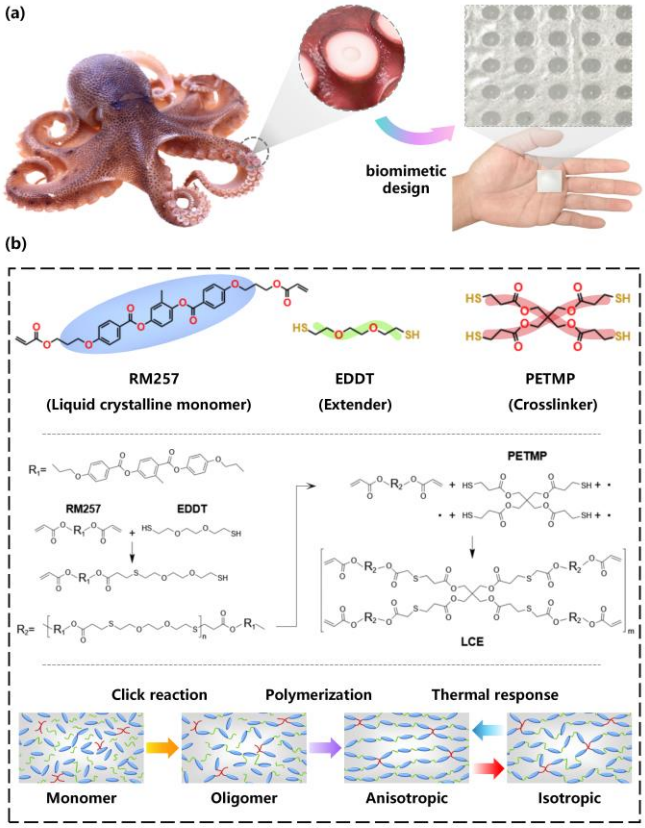

Figure 1. Illustrates the design and synthesis principles of S-LCE (a) Octopus-inspired structural design of S-LCE. (b) Synthesis reagents, chemical reaction process, and phase-transition mechanism of S-LCE.

II. Principle and Fabrication

A. Principle of the S-LCE Actuator

Octopuses possess unique tentacles densely covered with suckers, the chamber size of which can be precisely regulated by muscle contraction. This structural adaptation enables octopuses to firmly grasp objects underwater with remarkable flexibility. Unlike mammals, which typically rely on applying normal pressure with fingers to generate frictional forces for grasping, octopuses achieve secure adhesion by generating negative pressure at the sucker–substrate interface. This fundamental difference has attracted significant scientific

interest in the suction-based grasping mechanism of octopuses. However, most existing artificial octopus-inspired suckers rely on external air pumps to generate suction. In contrast, the liquid crystal elastomer (LCE) sucker actuator developed in this work mimics the contraction and relaxation of octopus muscles. The shrinkage and extension of polymer chains in LCE induce macroscopic chamber deformation, offering a mechanism of actuation that more closely replicates the biological principle of octopus suckers (Fig. 1a).

LCE exhibits two stable phases: the anisotropic nematic phase and the isotropic phase. Under thermal stimulation, LCE undergoes a reversible phase transition from anisotropic to isotropic, accompanied by pronounced dimensional and morphological changes. Upon removal of the stimulus, it reverts to the anisotropic state. This reversible thermally driven deformation makes LCE highly promising for actuator applications. The synthesis of S-LCE involves a three-step reaction: first, liquid crystal monomers and chain extenders undergo a thiol–acrylate Michael addition reaction to form oligomers (Fig. 1b). Subsequently, the LCE oligomers react with added crosslinkers through further thiol–ene Michael addition to yield a partially crosslinked network (Fig. 1b). Finally, UV irradiation triggers acrylate photopolymerization, producing a fully crosslinked LCE. Critically, the last step allows for molecular orientation programming: by applying a pre-stretch or stress field before UV curing, the alignment of mesogens is fixed into the polymer network, yielding anisotropic LCE. Such molecular orientation is essential, as it enables programmable actuation pathways under external stimuli, thereby tailoring performance to specific applications.

When anisotropic LCE is heated, it transitions to the isotropic state. This transformation arises from molecular-level interactions: in the anisotropic phase, mesogenic units containing biphenyl groups form π–π stacking interactions that stabilize ordered chain conformations at low thermal energy. Upon heating, the absorbed thermal energy increases intrachain bond energy, disrupting π–π stacking due to entropic effects and driving the polymer chains toward more disordered configurations. The collective molecular rearrangement during this transition leads to pronounced macroscopic deformation of LCE (Fig. 1b).

B. Synthesis Method of the S-LCE Actuator

The S-LCE material system was prepared using the following essential components: monomer, crosslinker, chain extender, catalyst, and photoinitiator. The liquid crystal monomer 1,4-bis[4-(6-acryloyloxyhexyloxy)benzoyloxy]-2-methylbenzene (RM257, Bidepharm, 95%), the dithiol chain extender 2,2′-(ethylenedioxy)-diethanethiol (EDDT, Macklin, 98%), and the tetrathiol crosslinker pentaerythritol tetrakis (3-mercaptopropionate) (PETMP, Macklin, 98%) were employed. Diphenyl-(2,4,6-trimethylbenzoyl)-phosphine oxide (TPO, Aladdin, 95%) was used as the photoinitiator, and dipropylamine (DPA, Aladdin, 95%) served as the catalyst. All reagents were used as received without further purification.

In the preparation process, RM257 (5 mmol) and the photoinitiator TPO (2 wt%) were dissolved in ethyl acetate (200 mg) and stirred at 70 °C for 15 minutes. A premixed solution containing the chain extender EDDT (3 mmol), crosslinker PETMP (1 mmol), and catalyst DPA (0.5 wt%) was then added, followed by vortex mixing for 5 minutes to ensure homogeneity. The resulting mixture was poured into a glass dish and cured at 85 °C for 12 hours via a thiol–ene click reaction, yielding isotropic LCE without applied orientation (Fig. 2a).

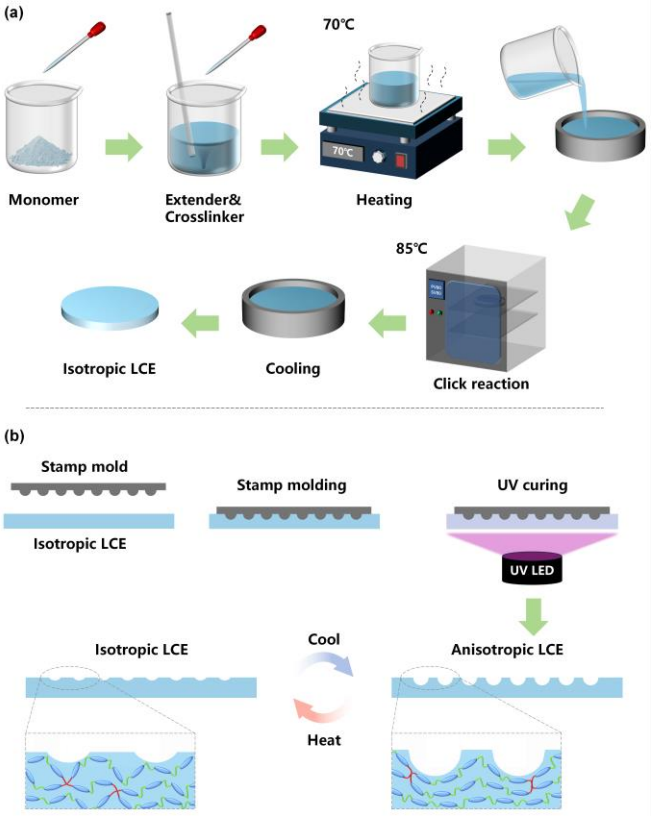

Figure 2. Fabrication and alignment process of S-LCE. (a) Chain extenders and crosslinkers are added to the mesogenic monomers and heated to complete the click reaction. (b) Stress alignment is applied to the LCE via an imprinting process, followed by UV irradiation to finalize the polymerization. The raised features of the stamp mold are transferred as cavities into the LCE, yielding an anisotropic S-LCE with concave chambers that shrink upon thermal stimulation as the material transitions to the isotropic state.

The isotropic LCE was processed via a stamp molding technique to obtain S-LCE with programmable geometries, endowing the material with highly versatile actuation capabilities. First, an acrylate-based stamp mold was fabricated using a Micro-LED 3D printer (Prismlab™ MP-36-3L) with a layer height of 5 μm. The mold surface featured an array of hemispherical protrusions (radius: 500 μm) spaced 500 μm apart. The stamp mold was pressed onto the surface of the isotropic LCE under a pressure of 10 kPa for 10 s. Subsequently, the assembly was exposed to 365 nm UV light for 15 minutes to cure the polymer. After removing the mold, anisotropic S-LCE with hemispherical cavities was obtained. Upon thermal stimulation, the anisotropic S-LCE transitioned to the isotropic state, causing a reduction in cavity volume (Fig. 2b).

III. RESULT

A. Physicochemical Properties of S-LCE

To verify the completeness of the UV-initiated acrylate polymerization (a critical factor, as complete polymerization

ensures that the programming orientation of the S-LCE is fully realized, with the cavity shape and size faithfully matching the imprint mold), Fourier transform infrared spectroscopy (FTIR, Bruker Vertex 70) was conducted before and after polymerization. As shown in Fig. 3a, the oligomer exhibited a distinct C=C stretching absorption peak at 1450 cm^{-1}, whereas this peak disappeared entirely in the fully polymerized sample. This confirms that the photopolymerization proceeded to completion, thereby maximizing the programmed orientation of the S-LCE.

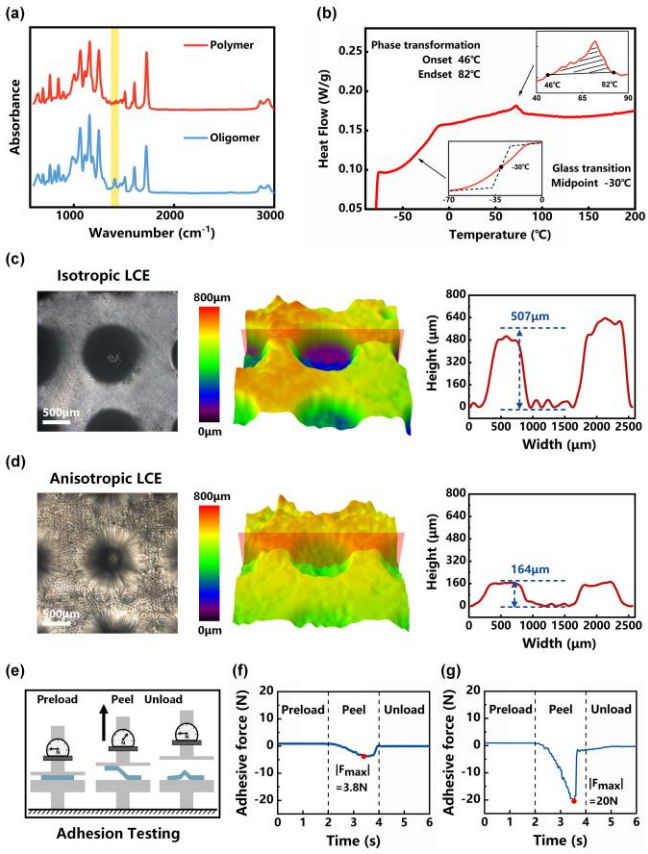

Figure 3. Physicochemical properties and transformation mechanisms of S-LCE. (a) FTIR spectra of S-LCE before and after polymerization. (b) DSC results of S-LCE. (c) Microscopic image, 3D reconstruction, and cross-sectional dimensions of anisotropic S-LCE. (d) Microscopic image, 3D reconstruction, and cross-sectional dimensions of isotropic S-LCE. (e) Schematic of the adhesion force testing system. (f) Maximum adhesion force of isotropic S-LCE. (g) Maximum adhesion force of anisotropic S-LCE.

The thermodynamic behavior of the S-LCE involves two characteristic transitions: the glass transition temperature common to polymers and the mesophase–isotropic transition unique to liquid crystal elastomers. To determine the transition temperature range, differential scanning calorimetry (DSC, NETZSCH DSC200F3) was performed. The results revealed a glass transition midpoint at –30 °C, while the anisotropic-to-isotropic transition initiated at 46 °C and was completed at 82 °C, as shown in Fig. 3b. This working temperature window renders the S-LCE highly suitable for grasping tasks in unmanned systems, as it provides a temperature range detectable by infrared cameras while avoiding interference with other onboard subsystems.

The working principle of the S-LCE, which mimics the suction mechanism of an octopus sucker, lies primarily in the temperature-dependent variation of its cavity volume. To investigate this behavior, both anisotropic and isotropic S-LCEs were examined and quantified using a laser confocal microscope (LEXT OLS5100). As shown in Fig. 3c, the anisotropic S-LCE exhibits a well-defined circular cavity structure. The left panel presents the optical micrograph, where the cavity and its edge contours are clearly visible. The middle panel shows the corresponding 3D reconstruction from laser scanning, in which a transverse cross-sectional line was extracted across the cavity center. The depth profile (right panel) reveals a maximum cavity depth of 507 μm, consistent with the designed height of the embossing mold, indicating that the mold geometry was faithfully transferred to the S-LCE and remained stable in its anisotropic state. Subsequently, the S-LCE was heated to 80 °C on a hot plate and re-examined under the confocal microscope. The results for the isotropic S-LCE are shown in Fig. 3d. In the left panel, the optical micrograph appears significantly brighter than in the anisotropic case, owing to the disordered molecular orientation in the isotropic state, which leads to enhanced optical transparency (a phenomenon widely exploited in liquid crystal displays). The circular cavity boundary appears blurred and tends to converge toward the center, reflecting a reduction in both cavity diameter and depth. The middle panel presents the 3D reconstruction, which confirms a pronounced cavity shrinkage. The cross-sectional profile, measured at the same location as in the anisotropic state (right panel), shows an average depth of 164 μm, substantially smaller than the initial 507 μm.

Taken together, the comparison between the anisotropic and isotropic states demonstrates that the S-LCE successfully emulates the working principle of an octopus sucker. Specifically, it achieves reversible cavity volume modulation without relying on external vacuum pumps or complex tubing, thereby enabling a simplified yet highly effective bioinspired adhesion mechanism.

The operational workflow of the S-LCE in grasping closely resembles that of an octopus sucker. First, the S-LCE is heated to its isotropic state, during which the cavity volume decreases. At this stage, the S-LCE is pressed against the surface of the target object with a predefined preload. Upon switching off the heating source, the temperature gradually decreases, inducing a phase transition of the S-LCE from the isotropic to the anisotropic state. This transition results in an expansion of the cavity volume, and due to the intimate contact with the object's surface, a negative-pressure vacuum is generated, enabling a firm and stable grasp on the target. The S-LCE can then perform subsequent manipulation tasks while maintaining this secure attachment. Once the operation is completed, reheating the S-LCE restores it to the isotropic state, leading to cavity shrinkage and the release of the target object as the negative pressure dissipates. Importantly, the isotropic S-LCE is immediately ready to undergo the next grasping cycle. This workflow is continuous, straightforward, and highly reliable, thereby offering excellent operational repeatability and robustness for practical applications.

We evaluated the adhesion performance of the S-LCE in both isotropic and anisotropic states. The schematic of the

testing system is shown in Fig. 3e. A high-precision rheometer equipped with a temperature-controlled module (Anton Paar 302e) was employed for the measurements. During the test, the S-LCE sample was first placed on the heating stage at 80 °C. The testing probe was then pressed against the S-LCE with a predefined preload to simulate the operational contact process. After removing the applied load, the S-LCE remained adhered to both the testing stage and the probe without external pressure interference. Subsequently, the probe was retracted vertically at a constant speed of 1500 μm/s, during which the S-LCE generated a counteracting tensile force that was precisely recorded. By conducting measurements at 30 °C and 80 °C, the adhesion forces exerted by the S-LCE under anisotropic and isotropic states, respectively, were quantified. The overall testing procedure is analogous to the flat-plate peel test commonly used for adhesives, thereby providing a reliable simulation of the adhesion behavior of S-LCE under practical working conditions.

Fig. 3f presents the adhesion force of the S-LCE at 80 °C. During the detachment stage, the maximum adhesion force generated by the S-LCE was only 3.8 N. Considering the tested S-LCE was a circular film with a diameter of 25 mm and a thickness of 1 mm, the calculated adhesion strength was merely 7741 Pa. This relatively weak adhesion strength enables the isotropic S-LCE at 80 °C to readily release the grasped object. In contrast, Fig. 3g shows the adhesion force of the S-LCE at 30 °C. In this case, the maximum adhesion force during detachment reached 20 N, corresponding to an adhesion strength of 40.7 kPa. This level of adhesion strength is sufficient to ensure stable grasping of most small- and medium-sized objects. The maximum load capacity is determined by the effective contact area between the S-LCE and the target surface; similar to an octopus, grasping larger objects requires multiple suction units operating in concert. A direct comparison between the adhesion strengths at 30 °C and 80 °C demonstrates that the S-LCE can reliably and accurately switch between strong adhesion for grasping and weak adhesion for release.

B. Adhesive Performance and Demonstration of S-LCE

Octopus suckers possess highly intricate internal architectures, owing to their ability to precisely regulate individual muscle fibers, which enables fine-tuned control of gripping forces. In contrast, the deformation of S-LCE is collective in nature, as the motion of individual polymer chains cannot be independently regulated. This raises the question of whether the cavity geometry of S-LCE significantly influences its adhesion strength. To investigate this, we designed three types of imprinting molds: in addition to the previously tested hemispherical cavity, cylindrical and conical geometries were also fabricated, and the corresponding S-LCE samples were prepared. The maximum adhesion forces at 30 °C were measured using the adhesion testing system described earlier. As shown in Fig. 4(a–c), the hemispherical S-LCE exhibited a maximum adhesion force of 20 N, the cylindrical cavity design reached 18 N, and the conical cavity yielded 19 N. All cavity structures shared a base radius of 500 μm and a depth of 500 μm, with glass substrates used as the adhered surface. Five repeated tests were performed for each case, and the deviation in maximum adhesion force was within 5%. These results indicate that cavity geometry exerts only a minor influence on the ultimate adhesion performance of S-LCE. We hypothesize that cavity depth may play a more significant role; however, during the experiments we observed that altering cavity depth inevitably increases the overall thickness of S-LCE. This has two major consequences: it slows down heat transfer, thereby reducing actuation response speed, and it also compromises the degree of deformation for cavities with large aspect ratios. For this reason, we selected cavities with a depth of 500 μm as the optimal design in the current study. Nevertheless, cavity architecture may hold the potential to enhance the overall performance of S-LCE, and we plan to explore this direction in future work.

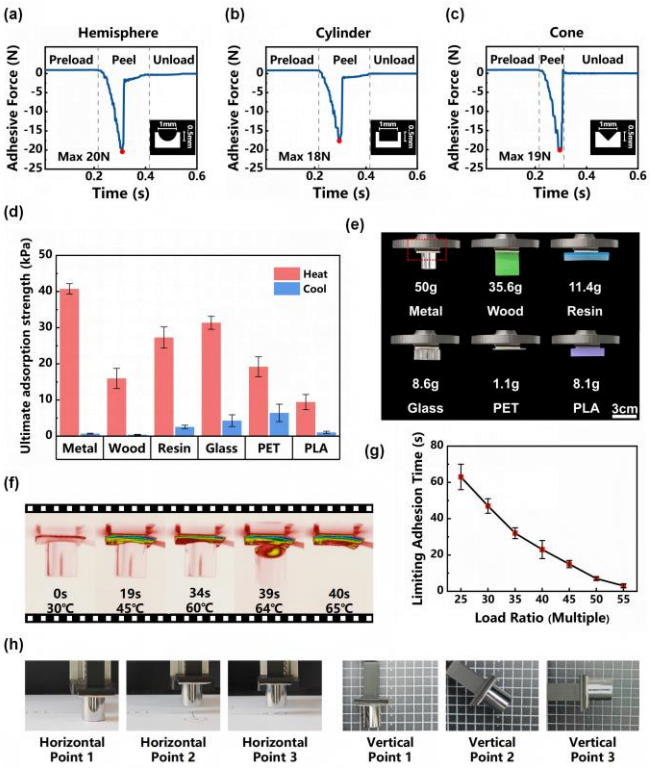

Figure 4. Factors influencing the performance and adhesion capability of S-LCE. (a) Maximum adhesion strength of S-LCE with a hemispherical cavity. (b) Maximum adhesion strength of S-LCE with a cylindrical cavity. (c) Maximum adhesion strength of S-LCE with a conical cavity. (d) High- and low-temperature maximum adhesion strength of S-LCE on different substrate materials. (e) Demonstration of S-LCE adhesion on various materials. (f) Infrared imaging of the S-LCE adhesion–release process. (g) Stable adhesion time of S-LCE as a function of its weight-to-load ratio. (h) Horizontal and vertical motion of objects grasped by S-LCE.

Building upon the hemispherical cavity structure of the S-LCE, we further evaluated its maximum adhesion strength on different substrate materials under both cold and heated states, as shown in Fig. 4d. Tests were conducted on metal, wood, resin, glass, PET, and PLA surfaces, and in all cases S-LCE exhibited a clear difference in maximum adhesion strength between the anisotropic (cold) and isotropic (heated) states. This indicates that S-LCE can reliably perform both grasping and releasing functions across a variety of material surfaces. Representative demonstrations of S-LCE grasping different surface objects are presented in Fig. 4e. To directly visualize the release process triggered by heating, we recorded an infrared thermal imaging video of S-LCE releasing a weight during a single cycle (Fig. 4f). As the temperature

increased, S-LCE transitioned from the anisotropic to the isotropic state, accompanied by a rapid decline in adhesion strength. The attached weight began to detach at approximately 64 °C, and complete release occurred in less than one second, highlighting the responsiveness of the system.

We further investigated the relationship between the self-weight of S-LCE and its adhesion strength by testing its ability to grasp and sustain loads with varying multiples of its own weight. The results showed that as the load increased, the maximum holding time decreased, indicating that excessive loads reduce the reliability of grasping. Finally, we demonstrated the practical grasping capability of S-LCE by manipulating it to grasp weights and move them in both horizontal and vertical directions (Fig. 4h). The stable performance observed for objects of appropriate mass confirms the significant potential of S-LCE as a lightweight and reliable end-effector for grasping tasks in unmanned systems.

IV. Conclusion

Based on experimental results and performance evaluations, the S-LCE actuator proposed in this work demonstrates significant advantages in achieving reversible, programmable, and lightweight adhesion without relying on external vacuum systems. The anisotropic-to-isotropic phase transition of the material enables rapid and reliable switching between strong adhesion (up to 40.7 kPa) and easy release, closely mimicking the muscle-driven mechanism of octopus suckers. Compared to most existing bioinspired suction systems, which typically depend on external pumps or complex fluidic circuits, the key innovation of S-LCE lies in its intrinsic stimulus-responsive actuation, allowing active control of adhesion and detachment. This fundamentally simplifies system architecture and enhances compatibility with soft and mobile robotic platforms, making it particularly suitable for constrained or dynamic environments such as aerial manipulation and underwater exploration.

The adhesion performance of S-LCE was found to be largely insensitive to the geometry of the cavities, which contrasts with certain bioinspired approaches that rely on finely optimized cavity structures to enhance sealing or adhesion strength. This study indicates that, for a driving mechanism based on phase-change-induced volumetric contraction, macroscopic material deformation rather than microscopic geometric features dominates the adhesion behavior. This finding offers a new perspective for simplifying the design of bioinspired suction cups. Nevertheless, cavity depth may influence the response speed and deformation efficiency, highlighting a trade-off between structural design and thermally driven performance. Future work could explore hierarchical or multi-scale cavity architectures, potentially combined with other strategies, such as surface micro-texturing to enhance wet adhesion or octopus-inspired lip-ring structures to improve sealing, to further optimize overall performance.

Furthermore, S-LCE exhibits stable and consistent adhesion performance across a wide range of substrate surfaces, including glass, metals, polymers, and wood, highlighting its remarkable surface insensitivity and environmental adaptability. The actuator demonstrates rapid thermal switching responses on the millisecond-to-second timescale, enabling controlled detachment within a very short period, and maintains excellent durability over more than 300 cycles with performance degradation below 5%, confirming its reliability and robustness in practical applications. Its overall lightweight structure, low driving energy consumption, and noise-free operation make it particularly suitable for advanced applications with stringent requirements on system weight, power, and silent operation, such as non-destructive handling of precision components, secure fixation in endoscopic surgical instruments, precise manipulation in on-orbit space maintenance, and efficient exploration and adhesion tasks for bioinspired robots in complex unstructured environments. Integration into the end effector of a robotic arm for full-cycle grasp–transport–release operations further demonstrate the practicality and system compatibility of S-LCE as a novel soft actuator. Although there remains room for optimization in large-scale arrayed coordination, energy efficiency, and long-term fatigue resistance—potentially through functional coatings or multi-physics actuation strategies—S-LCE undeniably offers a promising pathway to overcome reliance on traditional pneumatic and motor-based systems, establishing a solid material foundation for next-generation fully soft, self-powered, and intelligent robotic grasping systems.

Acknowledgment

This work was supported by the grants from the National Natural Science Foundation of China (No. 62303290, 52305325, 62373235), Shanghai Magnolia Talent Program Pujiang Project (23PJD036).

References

[1] J. Qu et al., “Recent Progress in Advanced Tactile Sensing Technologies for Soft Grippers,” Advanced Functional Materials, vol. 33, no. 41, Aug. 2023.

[2] D. J. Sut and P. Sethuramalingam, “Soft Manipulator for Soft Robotic Applications: a Review,” Journal of Intelligent & Robotic Systems, vol. 108, no. 1, May 2023.

[3] Stein van Veggel et al., “Classification and Evaluation of Octopus-Inspired Suction Cups for Soft Continuum Robots.” Advanced Science, vol. 11, no. 30, Jun. 2024.

[4] S. Baik, D. W. Kim, Y. Park, T.-J. Lee, S. Ho Bhang, and C. Pang, “A wet-tolerant adhesive patch inspired by protuberances in suction cups of octopi,” Nature, vol. 546, no. 7658, pp. 396–400, Jun. 2017.

[5] R. V. Martinez et al., “Robotic Tentacles with Three-Dimensional Mobility Based on Flexible Elastomers,” Advanced Materials, vol. 25, no. 2, pp. 205–212, Sep. 2012.

[6] W. Duan, Z. Yu, W. Cui, Z. Zhang, W. Zhang, and Y. Tian, “Bio-inspired switchable soft adhesion for the boost of adhesive surfaces and robotics applications: A brief review,” Advances in Colloid and Interface Science, vol. 313, p. 102862, Mar. 2023.

[7] J. Sun, L. Bauman, L. Yu, and B. Zhao, “Gecko-and-inchworm-inspired untethered soft robot for climbing on walls and ceilings,” Cell Reports Physical Science, vol. 4, no. 2, p. 101241, Feb. 2023.

[8] X. Wan et al., “Bioinspired chemical design to control interfacial wet adhesion,” Chem, vol. 9, no. 4, pp. 771–783, Mar. 2023.

[9] Shi, X.; Zhang, K.; Chen, J.; Qian, H.; Huang, Y.; Jiang, B. “Octopi Tentacles - Inspired Architecture Enables Self - Healing Conductive Rapid - Photo - Responsive Materials for Soft Multifunctional Actuators.” Advanced Functional Materials 2023, 34 (6).

[10] Z. Xie et al., “Octopus-inspired sensorized soft arm for environmental interaction,” Science robotics, vol. 8, no. 84, Nov. 2023.

[11] Z. Zhu et al., “Blue-ringed octopus-inspired microneedle patch for robust tissue surface adhesion and active injection drug delivery,” Science Advances, vol. 9, no. 25, Jun. 2023.
[12] M. Chen, L. Bai, H. Zheng, H. J. Qi et al., “Recent Advances in 4D Printing of Liquid Crystal Elastomers,” Advanced Materials, p. 2209566, Dec. 2022.
[13] Cui, B. et al., “Pretension-Free and Self-Recoverable Coiled Artificial Muscle Fibers with Powerful Cyclic Work Capability,”. ACS Nano 2023, 17 (13), 12809–12819
[14] Hebner, T. S.; Korner, K.; Bowman, C. N.; Bhattacharya, K.; White, T. J. “Leaping Liquid Crystal Elastomers,” Science Advances 2023, 9 (3).
[15] P. E. S. Silva, X. Lin, M. Vaara, M. Mohan, J. Vapaavuori, and E. M. Terentjev, “Active Textile Fabrics from Weaving Liquid Crystalline Elastomer Filaments,” Advanced Materials, p. 2210689, Feb. 2023.
[16] Yao, Y.; He, E.; Xu, H.; Liu, Y.; Yang, Z.; Wei, Y.; Ji, Y. “Enabling Liquid Crystal Elastomers with Tunable Actuation Temperature,” Nature Communications 2023, 14 (1)
[17] Song, C.; Zhang, Y.; Bao, Z.; Zhang, L.; Sun, J.; Lan, R.; Yu, Z.; Zhu, S.; Yang, H. “Light-Responsive Programmable Shape-Memory Soft Actuator Based on Liquid Crystalline Polymer/Polyurethane Network,”. Advanced Functional Materials 2023, 33 (17).
[18] L. Zhao et al., “Bio‐Inspired Soft‐Rigid Hybrid Smart Artificial Muscle Based on Liquid Crystal Elastomer and Helical Metal Wire,” Small, vol. 19, no. 17, Jan. 2023
[19] Y. Huang et al., “Photocontrollable Elongation Actuation of Liquid Crystal Elastomer Films with Well‐Defined Crease Structures,” Advanced Materials, vol. 35, no. 36, Jul. 2023.
[20] Z.-Z. Nie and H. Yang, “Structure‐induced Intelligence of Liquid Crystal Elastomers,” Chemistry: A European Journal, vol. 29, no. 38, Jun. 2023
[21] C. Chen et al., “Flexible and elastic thermal regulator for multimode intelligent temperature control,” SusMat, vol. 3, no. 6, pp. 843–858, Nov. 2023.
[22] S. Wu, Y. Hong, Y. Zhao, J. Yin, and Y. Zhu, “Caterpillar-inspired soft crawling robot with distributed programmable thermal actuation,” Science Advances, vol. 9, no. 12, Mar. 2023.
[23] Hu, Z. et al., "Springtail‐inspired Light‐driven Soft Jumping Robots Based on Liquid Crystal Elastomers with Monolithic Three‐leaf Panel Fold Structure," Angewandte Chemie International Edition, vol. 62, no. 9, Jan. 2023.
[24] S W. Hou, Jiaoyan Lv, et al., "Bioinspired Liquid Crystalline Spinning Enables Scalable Fabrication of High‐Performing Fibrous Artificial Muscles," Advanced Materials, vol. 35, no. 16, Mar. 2023